Supporting Information

A gating mechanism of pentameric ligand-gated ion channels

N. Calimet,[1] M. Simoes,[1] J.P. Changeux,[2,3] M. Karplus,[1,4] A. Taly,[5] and M. Cecchini[1,*]

[1]*ISIS, UMR 7006 CNRS, Université de Strasbourg, F-67083 Strasbourg Cedex, France*

[2]*CNRS, URA 2182, F-75015 Paris, France*

[3]*Collège de France, F-75005 Paris, France*

[4]*Department of Chemistry & Chemical Biology, Harvard University, 12 Oxford Street, Cambridge, MA 02138, U.S.A.*

[5]*IBPC, UPR 9080 CNRS, 75005 Paris, France*

Ion-pore closing

The atomistic and time-resolved description of the coupling between the position of P268 at the EC/TM domain interface and the size of the ion pore provided by the MD simulations sheds light on the structural details of the pore closing mechanism in GluCl. In particular, the simulation of GluCl with ivermectin removed suggests that the polar untilting of the M2 helices, which couples the repositioning of the interfacial loops to the closing of the pore, is realized through the coordinated *unbending* of the M2 and M3 helices; see Figure 4 in the *Main Text*. This conclusion is supported by the following observations. First, the C_α-RMSD of the M2 helix from the X-ray structure of GluCl after optimal superposition of M3 is significantly smaller than the deviation from the "locally closed" (LC) structure of GLIC [1] (Figure S6), which indicates that M2 and M3 move as a whole during the simulation and never un-couple as they do in the LC state. Second, the hydrogen-bonding pattern of M3 is permanently interrupted at residues 283 to 287 (Figure S8) due to the presence of a stable kink midway M3 (at residues M284-T285) which separates the third transmembrane helix into lower and upper segments that re-orient almost independently. Third, the upper part of M2 (residues 259 to 265) is surprisingly flexible and structurally less stable than the lower portion (residues 242-258). As shown by Figure S8, the probability distributions of the main chain H-bonding distances along M2 broaden significantly starting at residue 258 and reach values that correspond to loss of interaction (> 3.1 Å). In contrast to M3, however, the α-helical contacts in the upper part of M2 are only transiently lost and no permanent kink or hinge can be identified. Last, the polar tilting of the upper M2 is found to be significantly larger than that of the lower M2 and is strongly coupled to the position of P268 at the EC/TM interface; confront the time series of θ_p for the full-length, the upper

and the lower M2 with that of the V45-P268 distance in Figure S7. These observations indicate that also M2 is split into lower and upper segments, which facilitates the bending/unbending of the M2-M3 group; see cartoons in Figure S7. Importantly, the striking correlation between the inward displacement of the M2-M3 loop and the untilting of the upper M2 with little or no effect on the lower M2 (Figure S7) shows that the bending/unbending of the M2-M3 group is controlled by the position of P268 at the EC/TM interface. Thus, to maximize the signal to noise ratio while monitoring the tilting of the pore-lining helices in the simulation of GluCl, the polar tilting of the upper M2 rather than that of the full-length helix was considered; see Figure 3 in the *Main Text*.

Analysis of the α-helical contacts over the simulations of the prokaryotic channels shows that bending of M2 is also observed in GLIC but not in ELIC; see Figure S8. Strikingly, the location of the hinge region in the upper part of M2, which is the source of the transient loss of main chain H-bonding interactions during the simulations, is the same in GLIC and GluCl. The latter suggests that M2 bending is likely to be a general feature of the active state of pLGICs, which is lost on the transition to the resting state. The formation of more stable H-bonding interactions along M2 in the resting state is expected to increase the thermodynamic stability of the closed-channel form and is likely to contribute to the driving force for closing the ion pore. The distributions of the α-helical contacts along M3 for GLIC and ELIC are also shown in Figure S8. The hinge region in the middle of M3, which forms a stable kink in GluCl, is present in ELIC but not in GLIC. This feature, which mediates the bending/unbending of the M2-M3 group in GluCl, appears not to be exploited by the GLIC channel possibly due to its pH modulation that corresponds to a more delocalized perturbation. Perhaps the inherent rigidity of M3 in GLIC could be responsible for the structural separation of the M2 and M3 helices for closing the pore, which is observed in the structure of the locally closed state [1]. Taken together these results suggest that the bending/unbending of M2 is likely to be the tertiary change that couples the outward/inward displacement of the M2-M3 loop at the EC/TM interface to the opening/closing of the ion pore in pLGICs. In addition, we show that pore closing from the active state does not necessarily require the detachment of M2 from M3, as observed in the locally closed state of GLIC, although the latter could provide another mechanism for closing.

Given the length and the flexibility of the transmembrane helices in pLGICs, the structural definition of M2 was optimized to reduce the spread of the distributions of the tilt angle sampled by the simulations. In practice, an improved definition was obtained by discarding the intracellular portion of the helix (6 residues), which is structurally too unstable, and including the largest number of consecutive residues that corresponds to an integer multiple of the α-

helical pitch; i.e., as the pitch is equal to 3.6 residues, 17 over 24 residues (or 5 complete turns) were considered. This constrain optimizes the space distribution of residues on the plane perpendicular to the helical axis, thus reducing the noise in the determination of its absolute direction by least-square fitting of the C_α coordinates. These considerations have led to the following definitions of M2: residues 233 to 249 in ELIC, residues 227 to 243 in GLIC, and residues 248 to 264 in GluCl.

Agonist binding contacts in GluCl

The orthosteric neurotransmitter site of GluCl is located in the EC domain at the interface between subunits; see Figure S9. As described by Hibbs and Gouaux [2] the architecture of the site is box-like with loops from the (+) subunit forming the "sides" and residues from the β-strands of the (-) subunit defining the "base". In this arrangement, the C-loop defines the side of the pocket that is solvent exposed and adopts a fully closed or *shut* conformation. Interestingly, the crystal structure of GluCl makes it clear that the endogenous agonist bridges residues belonging to the rigid "core" of the (+) and (-) subunits thereby affecting their relative orientation; see Figure S9A.

The time evolution of the orthosteric site(s) of GluCl with ivermectin removed was analyzed by monitoring the agonist/receptor interactions over time, here referred to as *binding contacts*; see Figure S9B. The contact involving Y200 accounts for the cation-π interactions between L-glutamate and the C-loop of the receptor, which is considered to be crucial for agonist binding. Although cation-π interactions are not explicitly included in the energy model adopted here [3], previous calculations have shown that much of their effect is actually accounted for in classical force fields [4]. In the following, we first analyze the agonist/receptor contacts at subunits C/D and A/B to collect detailed information on the interactions that are key to stabilizing agonist binding. Then, we report on the behavior at the D/E and A/E subunit interfaces which yield insights on the coupling between agonist unbinding and the inward displacement of the M2-M3 loop.

C/D interface. At the C/D subunit interface the ligand stays bound to the orthosteric site throughout the trajectory and the C-loop remains closed. Nonetheless, the time series of the agonist/receptor contacts show the occurrence of an alternative binding mode that is sampled between 40 and 170 ns, as evidenced by the red traces on Figure S9B. The new binding mode corresponds to a small displacement of the ligand, which is sufficient to break the H-bonds with residues S150 and Y151 and reduce the contact with Y200. However, the salt-bridge interactions between the $\alpha-$ and $\gamma-$ carboxylate groups of L-glutamate and the positively charged residues

R37 and R56 on the (-) subunit as well as the vdW contact with Y151 on the (+) subunit are preserved. These interactions keep the ligand in place and prevent the opening of the C-loop.

A/B interface. At the A/B subunit interface, the C-loop opens rapidly by a large conformational change, which results in breaking of the H-bond with the backbone of residue Y151, a destabilization of the hydrogen bond with S150, and a strong reduction of the vdW contacts with residues Y200 and Y151; see corresponding black traces after 10 ns in Figure S9B. However, L-glutamate stays bound to the orthosteric site for ∼40 ns until a second rearrangement of the C-loop opens it. This rearrangement fully breaks the vdW contacts with the aromatic residues and the last backbone H-bond with the (+) subunit (S150). Strikingly, the unbinding of the agonist from the A subunit at ∼40 ns matches the inward displacement of the M2-M3 loop and the untilting of the M2 helix in the same subunit; see red traces of Figure 3 in the *Main Text*.

D/E interface. At the D/E interface, the analysis of the agonist/receptor interactions shows that L-glutamate unbinds from and rebinds to the (+) subunit twice during the simulation; see Figure S10. Interestingly, these unbinding/rebinding events have rather different consequences on the global structure of the receptor. In fact, the first unbinding, which occurs in about 20 ns as a consequence of a large rearrangement of the C-loop in the D subunit, correlates with no structural change at the EC/TM domain interface; see blue traces in Figure 3 in the *Main Text*. In sharp contrast, the second unbinding after 80 ns is coupled to the inward displacement of the M2-M3 loop as well as the polar untilting of the pore-lining helices. This surprising observation, i.e., that two similar rearrangements of the orthosteric site can have different allosteric consequences, indicates that agonist unbinding from the (+) subunit is not sufficient to elicit the shutting of the ion pore. Also, it suggests that the allosteric coupling between the chemical event (i.e., agonist binding/unbinding) and the functional conformational transition in the TM domain (i.e., ion-pore opening/closing) is indirect, so that a third element must be present to allow for effective structural communication. On the basis of the mechanism proposed here for gating, the quaternary twisting, which completes in ∼40 ns (Figure 2 in *Main Text*), is required for the allosteric coupling; see *Discussion*. This observation is in accord with the fact that agonist unbinding at 20 ns, i.e., before the twisting has completed, does not elicit an allosteric coupling, while the unbinding at 80 ns, i.e., after twisting has occurred, does.

E/A interface. At the E/A interface L-glutamate unbinds from the (+) subunit without affecting the conformation of the C-loop, which stays shut until the end of the simulation. In fact, after loosing all contacts with the (+) subunit, the ligand rebinds 6 Å away from the orthosteric pocket more down in the cleft. In the new binding mode, L-glutamate forms strong

electrostatic interactions with residues on the (-) subunit (R37, R56, and K171) and only weak vdW contacts with the C-loop (S193 and S195) and residues from the (+) subunit (P91 and F93). Nonetheless, the overall conformation of the orthosteric site remains stable. The surprising stability of the E/A interface may be explained by considering that the C-loop folds into a stable β-hairpin secondary structure after the repositioning of the agonist. This conformational change rigidifies the C-loop, which appears to be sufficient for mediating the structural communication between adjacent subunits on the simulation timescale. Intriguingly, these results suggest that the structural response of the receptor to agonist binding may be mediated by the conformation of the C-loop. In fact, when the C-loop populates its native β-hairpin fold, the structural communication between adjacent subunits becomes more efficient and even weaker *non-native* agonist/receptor interactions may stabilize the active or "bound" state of the receptor. The latter is expected to be even more relevant in the absence of agonist, as pLGICs have been shown to display non-zero basal activity [5]. Accordingly, residue substitutions that affect the β-hairpin propensity of the C-loop could be used to modulate the receptor sensitivity to agonist levels. Monitoring the basal activity of a series of mutants with engineered C-loops that span a range of β-hairpin propensities could provide experimental evidence for such an internal modulation mediated by a conformational transition of the C-loop.

Comparison with previous models of gating

In this section we compare the model of gating emerging from our simulations of GluCl (Figure 6 in *Main Text*) with previous experimental efforts to probe the sequence of structural events leading to activation/deactivation in pLGICs.

One model of gating based on electrophysiology recordings and double mutant cycle thermodynamic analyses of the human muscle acetylcholine receptor (AChR) was proposed by Lee *et al.* [6]. In this paper, site-directed mutagenesis was systematically performed at three residues at the EC/TM domain interface of the α-subunit, i.e., V46 on the β_1-β_2 loop, V132 on the Cys loop, and P272 on the M2-M3 loop, to analyze their contribution to gating. As the corresponding residues in GluCl play a central role in our model of pore closing, the comparison is pertinent. In short, Lee *et al.* found that: (i) residue substitutions at αP272, αV46, and αV132 result in quantitative changes of both the rate and equilibrium constants of gating, (ii) the substitution of the bulky side chains of either αP272 or αV46 by Glycine residues results in dramatic reductions of the dwell time in the open conformation (i.e., at least by one order of magnitude), (iii) these residues are strongly (energetically) coupled but contribute to ion-channel activation in a highly context dependent manner, as when V132 is mutated into

Alanine the coupling between αP272 and αV46 essentially disappears, and (iv) a triple substitution to Alanine residues (P272A-V46A-V132A) strongly suppresses channel gating, i.e., it reduces substantially the probability of populating the open-channel conformation even in the presence of agonist. Based on the low-resolution structure of the *Torpedo* AChR [7], which is supposed to represent a closed channel and shows that these residues are in contact, Lee *et al.* concluded that αP272, αV46, and αV132 are engaged in the closed-channel form, move together while approaching the transition state, and possibly disengage to reach the open-channel form. Therefore, they speculate that the EC domain acts as a brake to maintain the pore in the closed state and would allow channel opening through disengagement from the TM domain, which is opposite to what we propose based on the simulation analysis of GluCl.

The interpretation of Lee *et al.* has two weak points: (1) it is based on a low-resolution structure whose functional significance is still unclear, especially in light of the more recent cryo-EM reconstructions [8] obtained both in the presence (open) or the absence (closed) of ACh which look very similar (C_α-RMSD of 0.6 Å); and (2) it is inconsistent with the functional behavior of the triple mutant P272A-V46A-V132A, which is expected to favor and not suppress gating. Interestingly, the same data can be reinterpreted in light of the high-resolution structures of ELIC, GLIC and GluCl. Assuming that ELIC shows a closed-channel form, whereas GLIC and GluCl capture the open-channel form, the cryo-EM reconstruction of Unwin [7] appears to be closer to an open channel; i.e., the C_α-RMSD of the "core" is 2.4 Å with respect to GLIC/GluCl and 2.9 Å with respect to ELIC. The comparison is even more striking at the EC/TM domain interface where the C_α-RMSD of the M2-M3 helices after optimal superposition of the TM domain is 2.2 Å with respect to GLIC/GluCl and 3.1 Å with respect to ELIC. Similar conclusions were drawn by comparing the radius of the pore along the axis of the ion channel [9] or from the analysis of an MD trajectory of the *Torpedo* AChR structure, which clearly showed significant shrinking of the ion pore over time [10]. Interestingly, if this structure represented an active state, the weaknesses listed above would disappear and the interpretation of the data from Lee *el al.* would be consistent with our model. In fact, αP272, αV46, and αV132 would be considered to be engaged in the open state and disengaged in the closed state, which would explain the drop in the gating equilibrium constant in the triple Alanine mutant. Moreover, the absence of Cys-loop residues flanking the absolutely conserved Proline on the M2-M3 loop in GluCl is also consistent with no or low energetic coupling between the tip of the β_1-β_2 loop and the Proline on the M2-M3 loop, i.e., the tip of the β_1-β_2 loop provides a steric barrier for the movement of the M2-M3 loop in the direction of the ion pore. Taken together, these experimental data along with our computational results consistently point to a model where

the tip of the β_1-β_2 loop acts a brake for the inward displacement of the M2-M3 loop, whose interaction with the conserved Proline on the M2-M3 loop is controlled by agonist binding at the orthosteric site; see the *Main Text*.

Another model of gating in pLGICs has been proposed by Auerbach and coworkers based on a ϕ-value analysis of the murine AChR [11]. Based on an extensive set of mutants and corresponding electrophysiology recordings, these authors have determined ϕ-values for a large number of residues and have shown that amino acids with similar values of ϕ tend to cluster when mapped on the structure of the *Torpedo* AChR [12]. Also, the structural map of the ϕ-values revealed a spatial gradient going from the EC orthosteric site to the TM gate region. As ϕ-values can be used to measure the fractional time at which the mutated residues change their local environment from closed-like to open-like [13], Auerbach and coworkers proposed that ion-channel activation proceeds through a conformational "wave" that sequentially starts from the ligand-binding site (loops A, B, and C), propagates to the EC/TM interface (β_1-β_2 and Cys loops) and moves down to the transmembrane helices (first M2, then M4 and M3) to finally open the ion pore [11]. This model of activation was further corroborated by a calculated transition path based on coarse-grained normal-mode analyses of the structures of ELIC and GLIC [9]. Surprisingly, the mechanism emerging from our simulations of GluCl involves the same sequence of tertiary movements for closing rather than opening; i.e., the backward reaction. The apparent inconsistency points either to limitations of the temporal interpretation of ϕ, which neglects e.g. the existence of multiple pathways, intermediates, or hysteresis on the forward and backward paths, or the validity of the present allosteric model for pLGICs more generally. We note, however, that a straightforward interpretation of the ϕ-values in the backward direction (i.e., $1-\phi$) would suggest a mechanism for ion-channel deactivation that starts with the spontaneous closing of the pore while the agonist is still bound, produces rearrangements at the EC/TM interface as a consequence of the collapse of the M2 helices, and propagates to the orthosteric site destabilizing agonist binding. If this mechanism were correct, the closing rate would be essentially independent of the nature of the orthosteric agonist. In addition, the model of Auerbach and coworkers does not involve the quaternary twisting transition, which is a crucial step in our mechanism. Further studies are needed to resolve this issue.

---

* Corresponding author. Electronic address: mcecchini@unistra.fr

[1] Prevost MS, et al. (2012) A locally closed conformation of a bacterial pentameric proton-gated ion channel. *Nature Structural & Molecular Biology* 19:642–649.

[2] Hibbs R, Gouaux E (2011) Principles of activation and permeation in an anion-selective Cys-loop

receptor. *Nature* 474:54–60.

[3] MacKerell Jr A, et al. (1998) All-atom empirical potential for molecular modeling and dynamics studies of proteins. *The Journal of Physical Chemistry B* 102:3586–3616.

[4] Woolf T, Grossfield A, Pearson J (1999) Indoles at interfaces: calculations of electrostatic effects with density functional and molecular dynamics methods. *International Journal of Quantum Chemistry* 75:197–206.

[5] Jackson M (1984) Spontaneous openings of the acetylcholine receptor channel. *Proceedings of the National Academy of Sciences* 81:3901–3904.

[6] Lee W, Free C, Sine S (2008) Nicotinic receptor interloop proline anchors β1-β2 and Cys loops in coupling agonist binding to channel gating. *The Journal of General Physiology* 132:265–278.

[7] Unwin N (2005) Refined structure of the nicotinic acetylcholine receptor at 4Å resolution. *Journal of Molecular Biology* 346:967–989.

[8] Unwin N, Fujiyoshi Y (2012) Gating movement of acetylcholine receptor caught by plunge-freezing. *Journal of Molecular Biology* 422:617–634.

[9] Zheng W, Auerbach A (2011) Decrypting the sequence of structural events during the gating transition of pentameric ligand-gated ion channels based on an interpolated elastic network model. *PLoS Computational Biology* 7:e1001046.

[10] Liu X, et al. (2008) Mechanics of channel gating of the nicotinic acetylcholine receptor. *PLoS Computational Biology* 4:e19.

[11] Auerbach A (2010) The gating isomerization of neuromuscular acetylcholine receptors. *The Journal of Physiology* 588:573–586.

[12] Purohit P, Mitra A, Auerbach A (2007) A stepwise mechanism for acetylcholine receptor channel gating. *Nature* 446:930–933.

[13] Auerbach A (2007) How to turn the reaction coordinate into time. *The Journal of general physiology* 130:543–546.

[14] Nury H, et al. (2010) One-microsecond molecular dynamics simulation of channel gating in a nicotinic receptor homologue. *Proceedings of the National Academy of Sciences* 107:6275.

Supporting Tables

TABLE S1: Residue flips predicted by Molprobity for ELIC (2VL0, 40 flips) and GluCl (3RIF, 26 flips). No flips were predicted for GLIC (3P50).

	ELIC		GluCl	
Domain	Residue	In chain(s)	Residue	In chain(s)
EC	Gln42	B, C, E	Asn46	A, B, C, D, E
	Gln62	A, B, C, E	Gln84	A, B, C, D, E
	Gln124	A, B, C, D, E	His101	A, C, D, E
	Asn151	A, B	Gln169	A, B, C, D, E
	Asn154	A, B, E		
	His176	E		
	Gln184	A, D, E		
	Asn185	A, B, C, D, E		
	Asn199	A, B, C, D, E		
TM	Gln232	C	Gln219	C, D
	His283	C	Gln259	A, B, C, D, E
	Gln286	B, D		
	Gln297	A, B, C, D, E		

TABLE S2: Definitions of the "core" residues of ELIC, GLIC, and GluCl that form the evolutionary conserved topology of pLGICs. For each ion channel residue numbering follows that of the corresponding crystal structure, which is given in parenthesis. The secondary structure motifs forming the "core" are also listed.

Domain	Motif	ELIC (2VL0)	GLIC (3P50)	GluCl (3RIF)
EC	β_1	13–24	17–28	29–40
	β_2	32–43	36–47	48–59
	β_6	100–111	100–111	118–129
	β_7	123–132	123–132	141–150
	β_{10}	189–197	183–191	202–210
TM	M1	205–222	199–216	218–235
	M2	227–250	221–244	242–265
	M3	259–284	253–278	274–299
	M4	300–316	296–312	320–336

TABLE S3: Definitions of the *core* residues for the human muscle nAChR relative to GluCl.

Domain	Motif	GluCl (3RIF)	nAChR (4AQ5)
EC	β_1	29–35	30–36
	β_2	53–59	54–60
	β_6	118–123	116–121
	β_7	141–150	139–148
	β_{10}	202–210	200–208
TM	M1	218–235	216–233
	M2	242–265	243–266
	M3	274–299	275–300

TABLE S4: Residues in GluCl and GLIC predicted to deviate from their standard protonation state. All ELIC titratable groups are predicted in their standard state at pH 7.

	Residue	[a] Model pK_a	[b] Predicted pK_a	Target pH	
		in solution	in protein	[c] Populations (%)	State (charge)
				pH 4.5	
GluCl	Glu 57	4.4	>16	100; 0	protonated (0)
	Asp 277	4.0	[d] n/a	53; 47	protonated (0)
	Glu 293	4.4	>16	100; 0	protonated (0)
	[e] His 101	7.0	<-2	10; 62; 28	protonated on Nδ1 (0)
				pH 4.6	
[f] GLIC	His 127	7.0	9.7	100; 0; 0	doubly protonated (+1)
	His 235	7.0	<-2	0; 1; 99	protonated on Nϵ2 (0)
	His 277	7.0	4.8	55; 16; 29	doubly protonated (+1)

[a] Reference pK_a for the side chain titratable group.

[b] pH at which the protonation probability is one-half.

[c] Acid and base forms; Histidines: (+1) imidazolium ion; (neutral) imidazole Nδ1 tautomer; (neutral) imidazole Nϵ2 tautomer.

[d] Multiple half-protonation points resulting from non-sigmoidal behavior of the titration curve; the ionization state was chosen according to the relative populations at the given pH.

[e] All the other His residues are predicted as positively charged.

[f] Glutamic acids 26, 35, 67, 69, 75, 82, 177, 243 and Aspartic acids 86, 88 were considered in their protonated forms as done in Ref. [14].

Supporting Figures

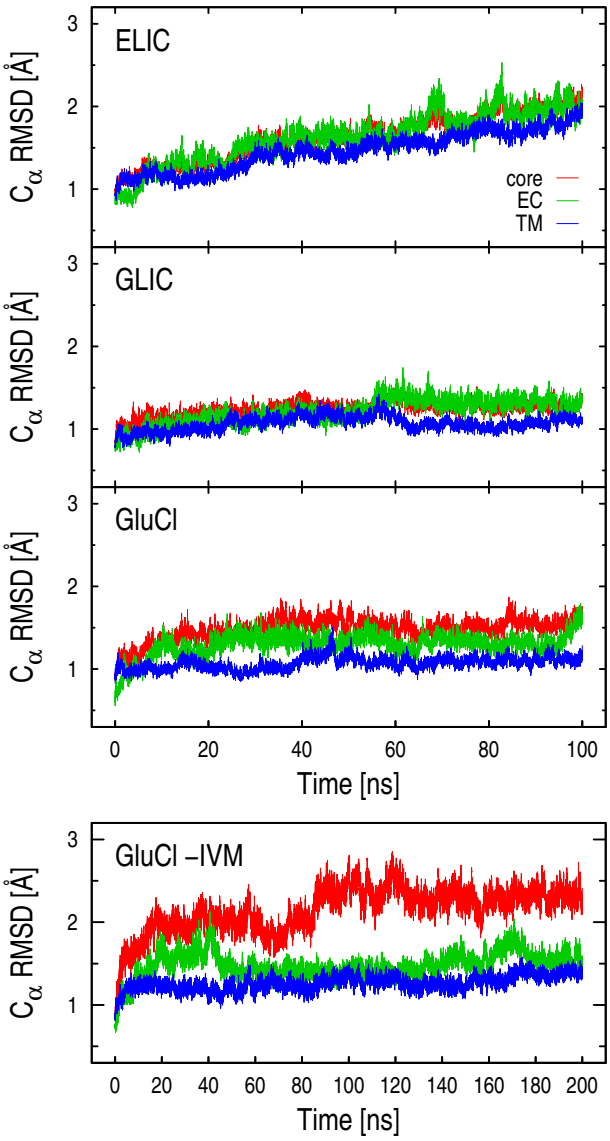

FIG. S1: Time series of the C_α-RMSD from the X-ray structure of ELIC, GLIC, and GluCl with and without ivermectin. The structural evolution of the universally conserved "core" (see Table S2) is shown in red, the deviation of the EC and TM core residues from the crystal are given in green and blue, respectively. The structures of GLIC and GluCl fluctuate very close to their starting conformations as shown by average RMSD values for the C_α atoms of the "core" of 1.2 and 1.5 Å, respectively. The conformation of ELIC is also preserved on the simulation timescale although it deviates more from the X-ray structure with an average RMSD of 1.6 Å. In sharp contrast, the conformation of GluCl with ivermectin removed (-IVM) rapidly evolves to a new structural state as evidenced by a sudden increase of the RMSD over the first 20 ns, followed by a second jump between 60 and 100 ns. Interestingly, the much smaller values of the RMSD for both the EC (average RMSD of 1.4 Å) and TM (average RMSD of 1.2 Å) domains indicate that the large structural deviation observed in the absence of ivermectin originates from the EC and TM domains repositioning one relative to the other.

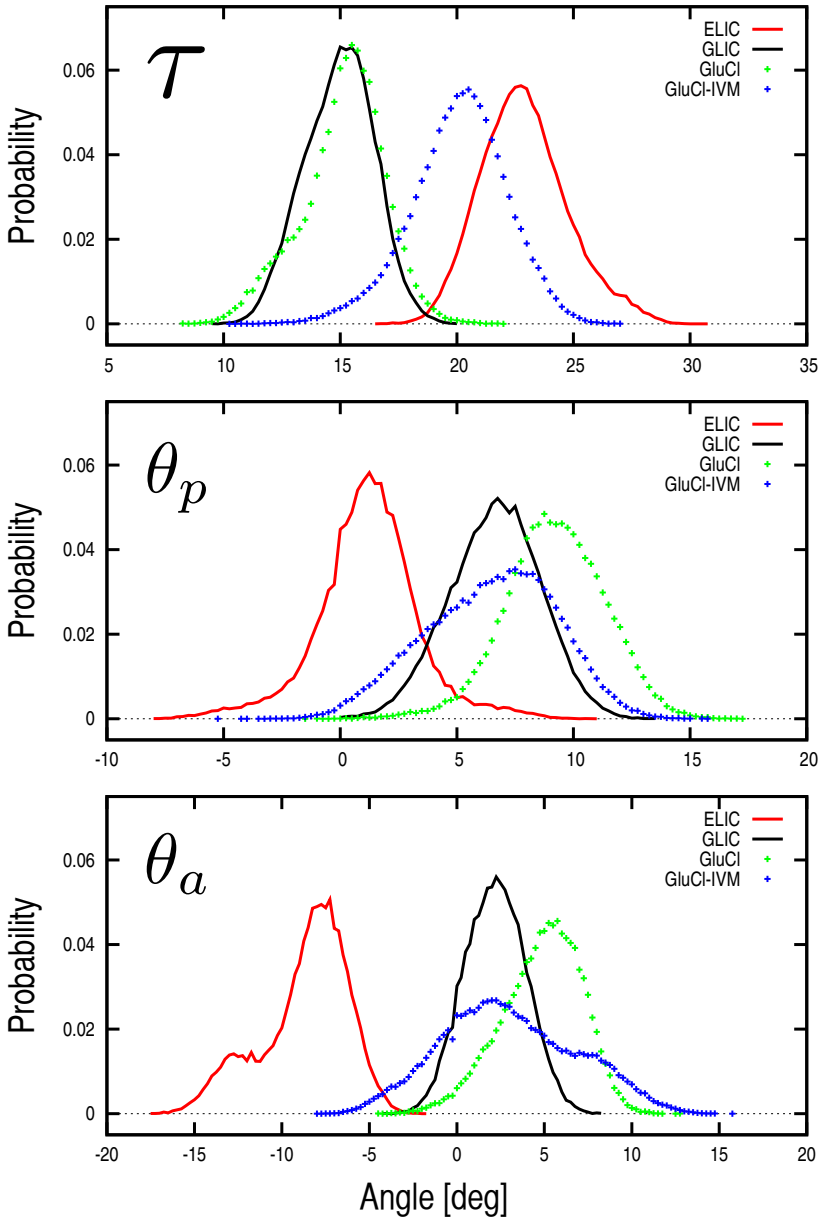

FIG. S2: Probability distributions of the structural observables. The normalized histograms of the twist (τ) and the polar and azimuthal M2 tilting components (θ_p, θ_a) sampled by the simulations of ELIC, GLIC and GluCl in the presence or the absence of ivermectin are shown in red, black, green and blue, respectively. The probability distributions were determined after merging the time series of the observables collected for the individual subunits; this post averaging makes it possible to include the contributions of individual conformational transitions that would be averaged out by pre-averaging. The room-temperature distributions of the various observables show that there is little overlap between the resting (ELIC) and the active state (GLIC or GluCl with ivermectin bound) of the ion channel. Interestingly, upon removal of ivermectin the distribution of the twisting (τ) and the M2 polar tilting (θ_p) of GluCl shift towards values which are typical for the resting state; compare the overlap between the red with the green (+IVM) and the blue (-IVM) distributions. By contrast, the distribution of the M2 azimuthal tilt (θ_a) show no significant overlap with the resting state.

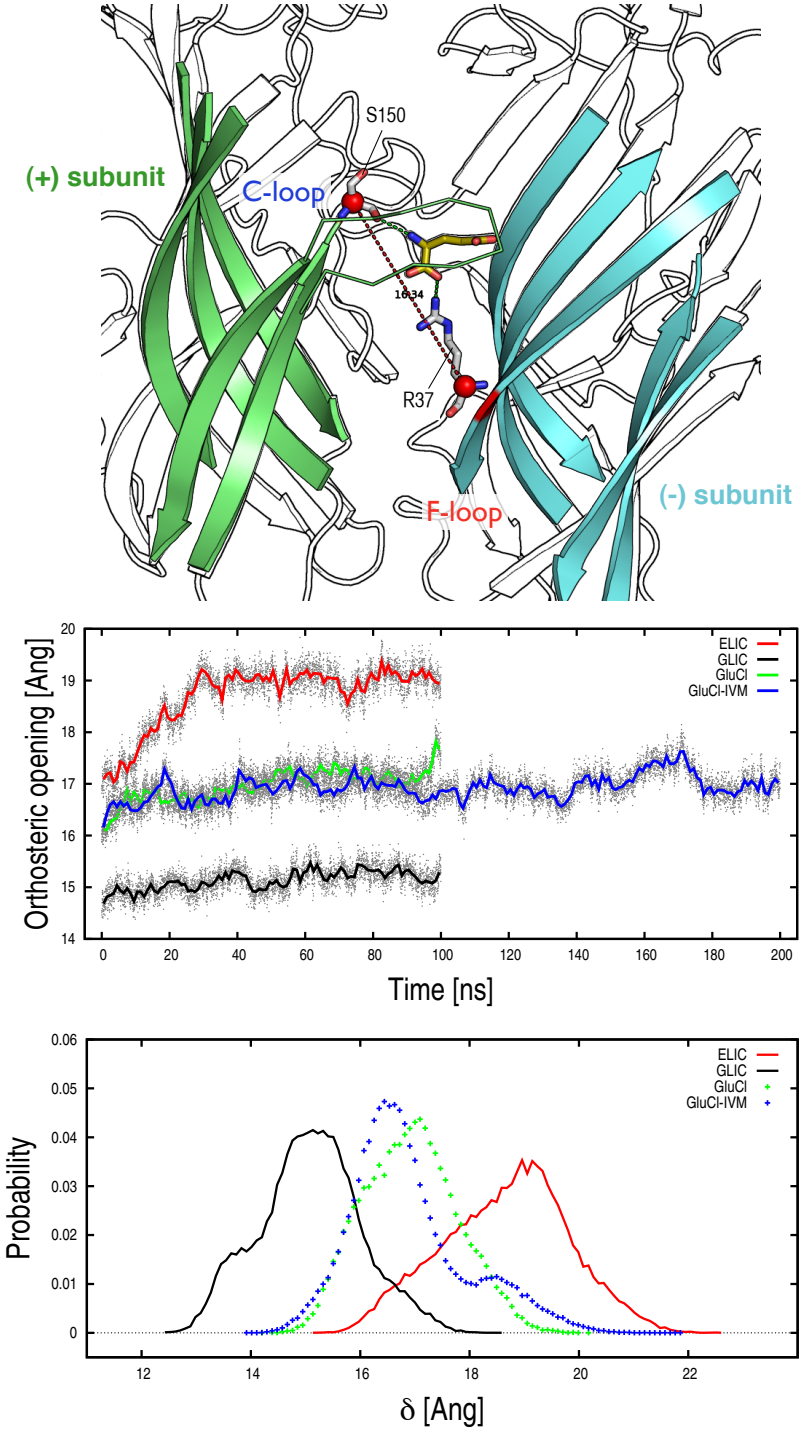

FIG. S3: Orthosteric site opening in pLGICs. On top, a cartoon representation of δ based on the X-ray structure of GluCl is given. The β-sandwiches forming the structurally conserved *core* of the principal (+) subunit and the complementary (-) subunit are shown as cartoons and colored in green and cyan, respectively. The residues involved in the definition of δ, i.e., S150 and R37 in GluCl, are shown as sticks with the position of the C_α atoms highlighted by red balls. The endogenous agonist L-glutamate bound at the orthosteric site is colored in yellow. The figure makes clear that S150 and R37 belong to the structurally conserved *core* of the EC domain, they define approximately the position of the C-loop and the F-loop at the subunits interface and form H-bonding interactions with the agonist. In the middle and on bottom, the time series of the average δ and the probability distributions for the individual subunits sampled by the room temperature simulations of ELIC, GLIC, and GluCl with and without ivermectin are shown in red, black, green and blue, respectively. Despite a large difference between the opening of the orthosteric site of GLIC (15 Å) and ELIC (19 Å), the data show that the observable δ does not distinguish between the simulations of GluCl with and without ivermectin.

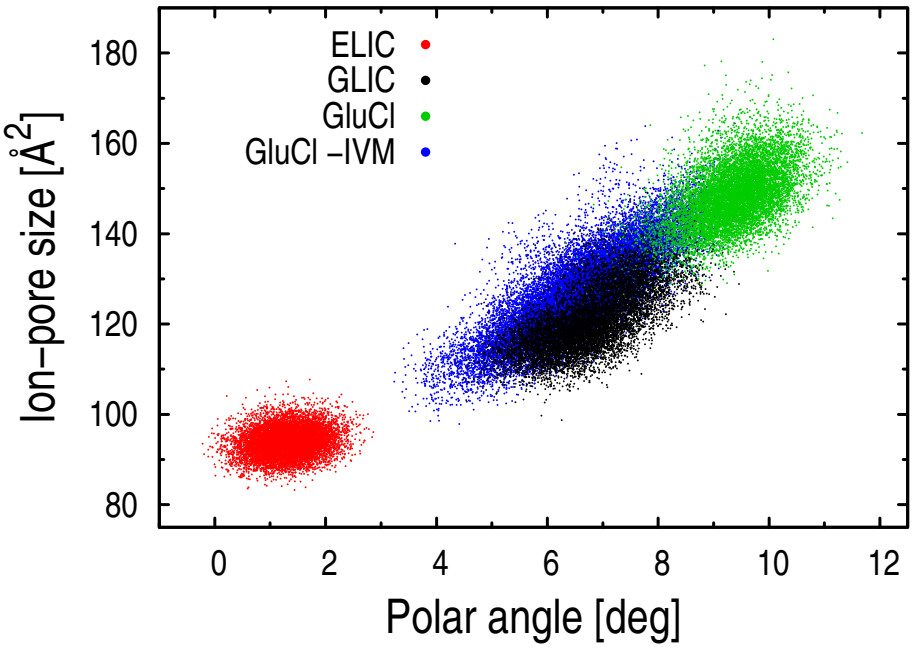

FIG. S4: Correlation between the size of the ion pore at the constriction point (σ) and the M2 polar tilting (θ_p) during the simulations of ELIC, GLIC and GluCl with and without ivermectin (IVM). Data points correspond to the time series of σ and θ_p shown in Figure 2 of the *Main Text*. The distributions show a strong correlation in GluCl without ivermectin (blue dots, 0.82), a weaker correlation in GluCl with ivermectin present (green dots, 0.54) and GLIC (black dots, 0.63), and essentially no correlation in ELIC (red dots, 0.17); the value of correlation coefficient is given in parenthesis. The similar slope of the black, green, and blue distributions indicate that the TM domain of GLIC and GluCl with and without IVM have a similar dynamic behavior, which is markedly different from that of ELIC. Moreover, the larger spread of the blue distribution relative to the black and the green ones indicates that the removal of IVM lowers significantly the energy required for closing. Altogether, these results show that the functional vibrational modes of the TM domain are conserved in the active state of the channel but that their frequency is modulated by agonist binding, i.e., IVM in GluCl and pH in GLIC.

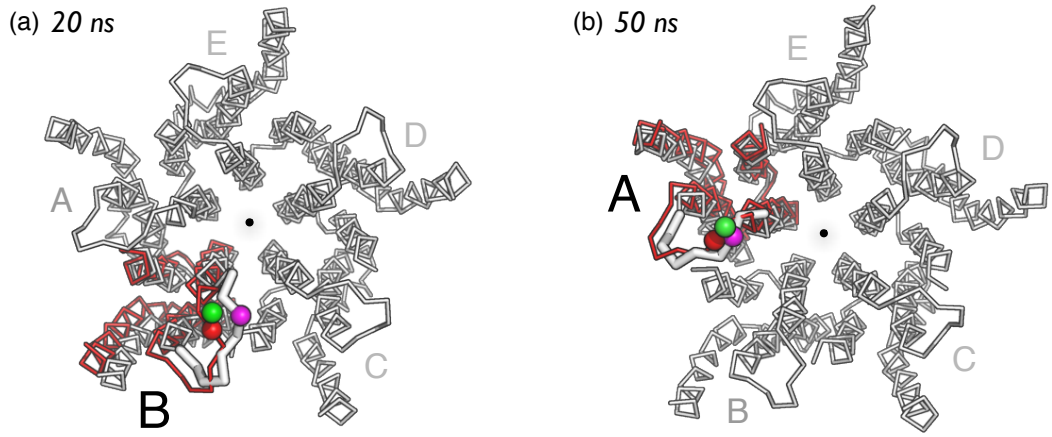

FIG. S5: Tangential displacement of the M2-M3 loop sampled by the B subunit of GluCl in the absence of ivermectin at 20 ns. Snapshots of the TM domain taken from the simulation at (a) 20 ns and (b) 50 ns are shown in white, that of the crystal structure is in red. The initial position (X-ray) of the C_α atoms of V45 (β_1-β_2 loop) and P268 (M2-M3 loop) are shown by green and red spheres, respectively. Magenta spheres indicate the position of the C_α atom of P268 at 20 ns for subunit B and 50 ns for subunit A. The conformation of the M2-M3 loop in the A and B subunits is highlighted by a thick white tube. The comparison with the crystal structure shows that the similar increase in the V45-P268 distance measured at 20 and 50 ns in the B and A subunits, respectively, actually correspond to rather different rearrangements. In fact, while the former monitors a tangential repositioning of the M2-M3 loop with respect to the β_1-β_2 loop, the latter corresponds to a radial displacement of the M2-M3 loop in the direction of the ion pore, which is referred to as an *inward displacement*. This analysis shows that the signal measured in the B subunit at 20 ns (see green dotted line in Figure 3A in the *Main Text*) is spurious. Therefore, no inward displacement of the M2-M3 loop is sampled before the global twisting of the ion-channel completes.

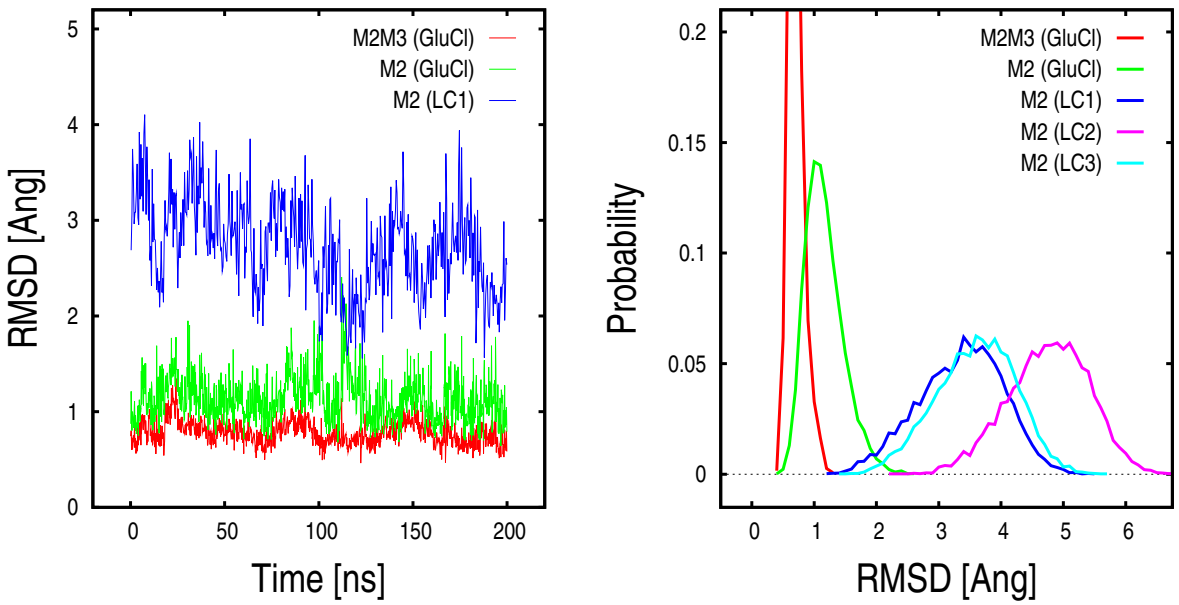

FIG. S6: Structural coupling between the transmembrane helices M2 and M3 during the simulation of GluCl with ivermectin removed. On the left, time series of the C_α-RMSD of: M2 and M3 after best-fit to the X-ray structure of GluCl (red); M2 only after optimal superposition of M3 to GluCl (green) and the locally closed (LC) state of GLIC (blue). Data points refer to subunit A only. On the right, the corresponding probability distributions are shown. For completeness, the structural comparison with the LC state was made using one representative structure per subtype following the classification given in Ref. [1]: 3TLU for LC1, 3TLW for LC2, and 3TLV for LC3. The data show that independent of the polar untilting transition sampled by subunit A at 42 ns (see Figure 3 in the *Main Text*), M2 and M3 move as a whole during the simulation and never detach as seen in the LC state of GLIC.

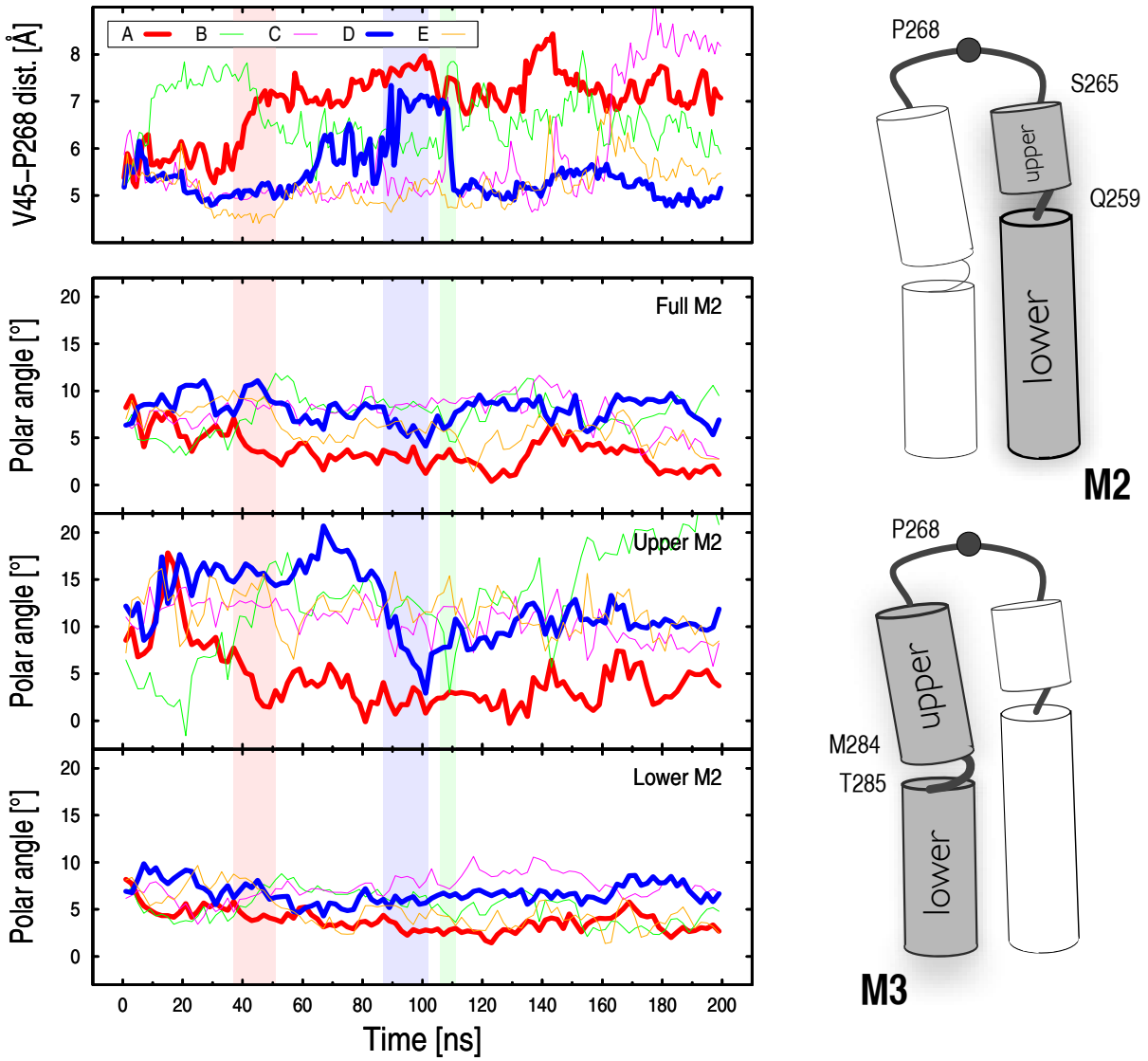

FIG. S7: The polar tilting of the upper M2 helix is controlled by the position of P268 at the EC/TM domain interface. The time series of the polar tilting of the full-length M2 (residues 248-264), the upper M2 (residues 259-265) and the lower M2 (residues 242-257) are compared to the time evolution of the distance between the interfacial residues V45 (β_1-β_2 loop) and P268 (M2-M3 loop). Data points correspond to time averages taken over consecutive windows of 1 ns (i.e., 50 snapshots). In the background, light red, light blue, and light green regions mark the time span of the inward displacement of the M2-M3 loop in the A, D, and B subunits, respectively. The data highlight a striking time correlation between the inward displacement(s) of the M2-M3 loop, which correspond to a large increase in the V45-P268 distance, and the untilting of the upper M2 helix. In sharp contrast, the orientation of the lower M2 is essentially independent of the position of the M2-M3 loop. Taken together with the data reported in Figures S8 and S6 these results indicate that both transmembrane helices M2 and M3 are separated into a lower and an upper segments, which re-orient almost independently. The upper part of the two helices are structurally coupled and move as a whole. As the orientation of the upper M2 is controlled by the position of P268 at the EC/TM domain interface, the repositioning of the M2-M3 loop relative to the β_1-β_2 loop at the EC/TM domain interface drives the bending/unbending of the M2-M3 group, which allosterically couples the inward displacement of the M2-M3 loop to the closing of the ion pore.

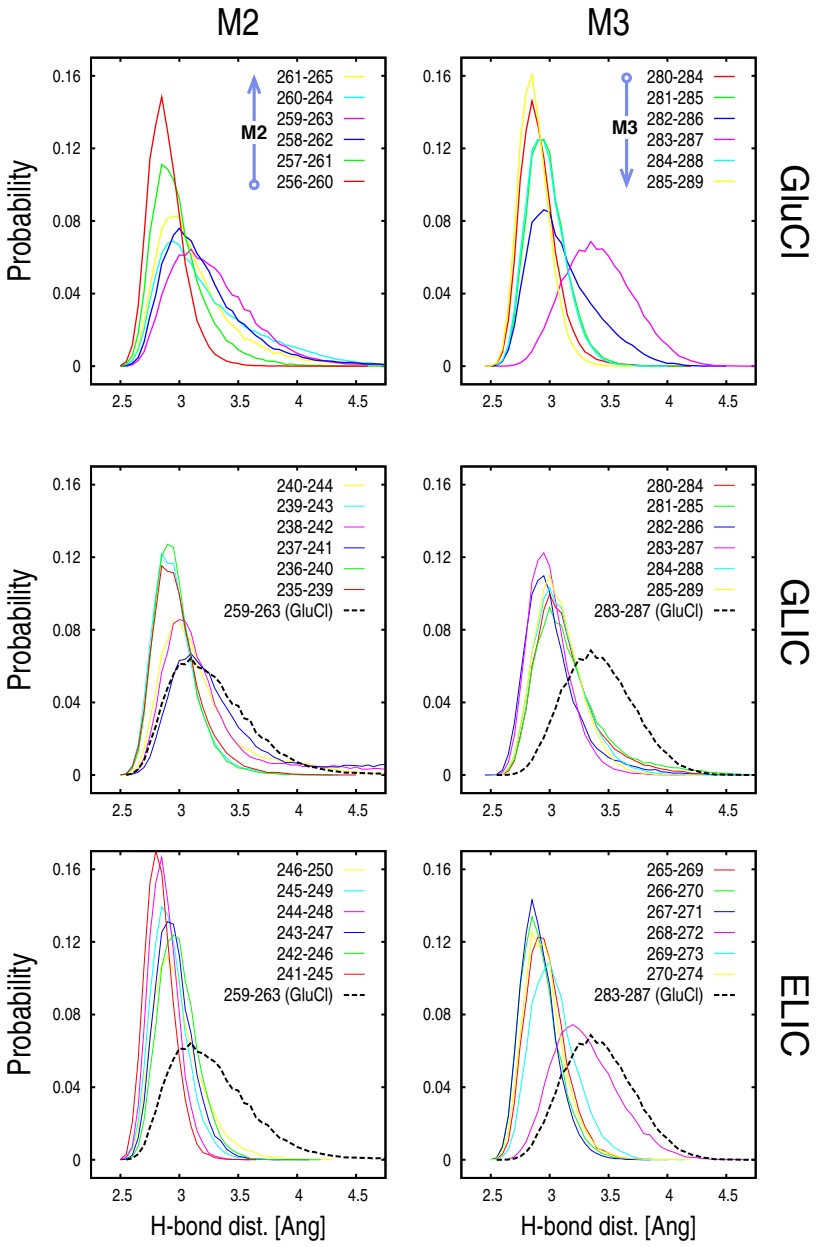

FIG. S8: The transmembrane helices M2 and M3 are structurally separated into lower and upper segments in the active state of GluCl. The room-temperature probability distributions of the main chain H-bond distances monitored along M2 and M3 are shown for GluCl, GLIC and ELIC on the left and the right-hand side, respectively. H-bonding distances were determined by measuring the separation between the carbonyl oxygen of residue i and the amide nitrogen of residue $i+4$ along the simulation trajectory. For GluCl, the analysis shows that starting at residue 258, the α-helical contacts in the upper part of M2 are transiently lost during the simulation (on top, left). In addition, the distributions along M3 indicate that the H-bonding pattern is permanently interrupted at residues 283-287 (on top, right), which shows the presence of a stable helical kink or hinge at residues M284 and T285. The separation of both transmembrane helices into upper and lower regions, which may re-orient almost independently, greatly facilitates the bending/unbending of the M2-M3 group in the active state. In GLIC, the analysis of the α-helical contacts shows that the bending of M2 is preserved; compare the distribution of the H-bond distance at residues 237-241 in GLIC (blue) with that at residues 259-263 in GluCl (black dashed line) on the left. By contrast, no hinge or kink is observed in M3 (middle, right). Finally, in ELIC a hinge region in the in the middle of M3 is consistently observed at residues 268-272 (on bottom, right) but no flexibility in M2 is detected (on bottom, left).

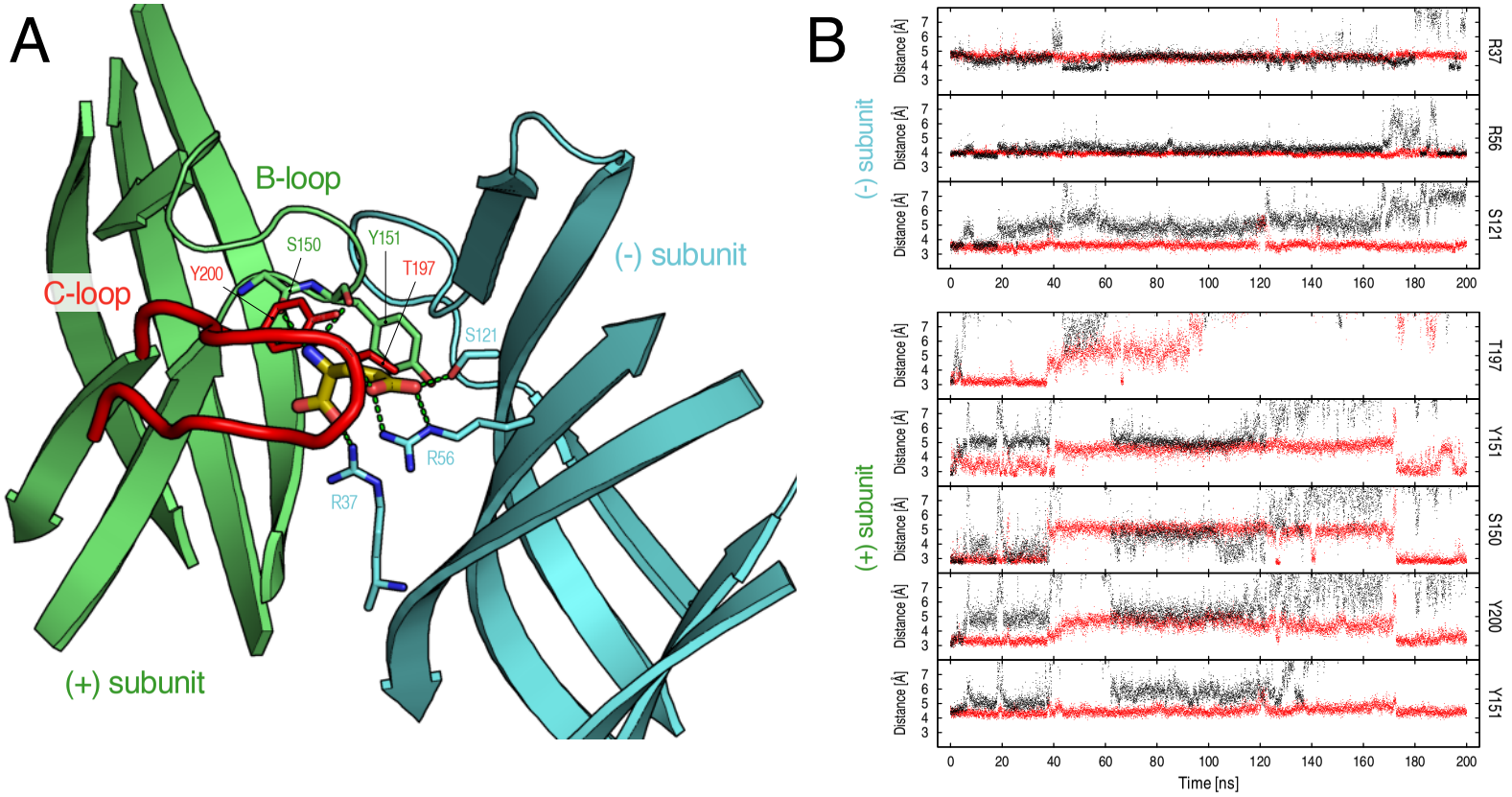

FIG. S9: Analysis of the agonist binding contacts along the simulation of GluCl with ivermectin removed. (A) The orthosteric neurotransmitter site in the crystal structure. The structural core of the principal (+) and the complementary (-) subunits are shown in green and cyan, respectively; the C-loop is in red and the endogenous agonist, here L-glutamate, is in yellow. Several interactions stabilize the bound conformation of the agonist: the $\alpha-$ and $\gamma-$ carboxylate groups make strong H-bonds with the positively charged R37 and R56 on the (-) subunit and polar interactions with the hydroxyl group of S121 on the (-) subunit and T197 on the C-loop of the (+) subunit; the position of the α amino nitrogen is stabilized by a cation-π interaction with Y200 on the C-loop and two hydrogen bonds with the main chain carbonyl oxygens of S150 and Y151 on the B-loop of the (+) subunit; vdW contacts with the side chain of Y151 and other residues on the C-loop complete the interaction pattern. All residues contributing to agonist binding are shown as sticks. (B) Time evolution of the agonist/receptor contacts. Binding contacts were analyzed by measuring, from top to bottom, the distance between the $\alpha-$ and $\gamma-$ carboxylic carbons of the agonist with the carbon atoms of the guanidinium group of R37 and R56 or the oxygen atoms of the hydroxyl group of S121 and T197; the distance between the α-amino nitrogen of L-glutamate with the backbone oxygens of S150 and Y151 or the side chain of Y200; and the distance between the center of mass of the agonist and the side chain of Y151. The first three define binding contacts with the (-) subunit, the latter five contacts with the (+) subunit. Traces corresponding to binding contacts at the C/D interface are shown in red, those at the A/B interface are given in black.

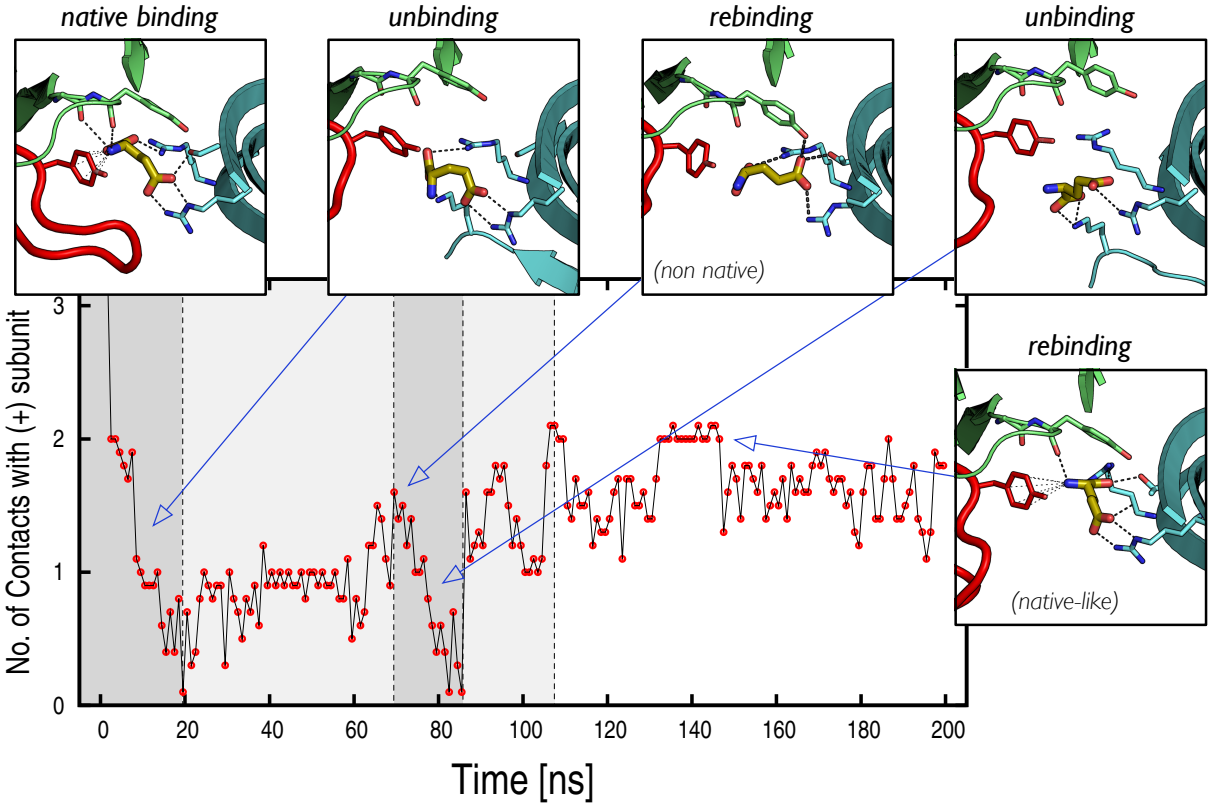

FIG. S10: Agonist unbinding/rebinding at the D/E interface of GluCl with ivermectin removed. The time series of the number of native contacts of the endogenous agonist with the (+) subunit is shown. Contacts were counted if the distance between the centers of mass of the ligand and the side chain of any residue belonging to the D subunit was less than 6.5 Å. Data points correspond to averages taken over consecutive time windows of 1 ns (i.e., 50 snapshots). In the background, dark and light gray is used to show time spans corresponding to L-glutamate unbinding and rebinding, respectively. On top and on the aside, snapshots taken along the trajectory complement the analysis with a structural representation of the ligand/receptor interactions at the orthosteric site. The sequence of images shows that after the first unbinding from the (+) subunit, the salt-bridging interactions with residues on the (-) subunit (R37, R56, and K171) keep the agonist in place such that it can rebind to the (+) subunit through non-native interactions; i.e., a strong hydrogen bond between the $\gamma-$ carboxylate and the hydroxyl group of Y200.

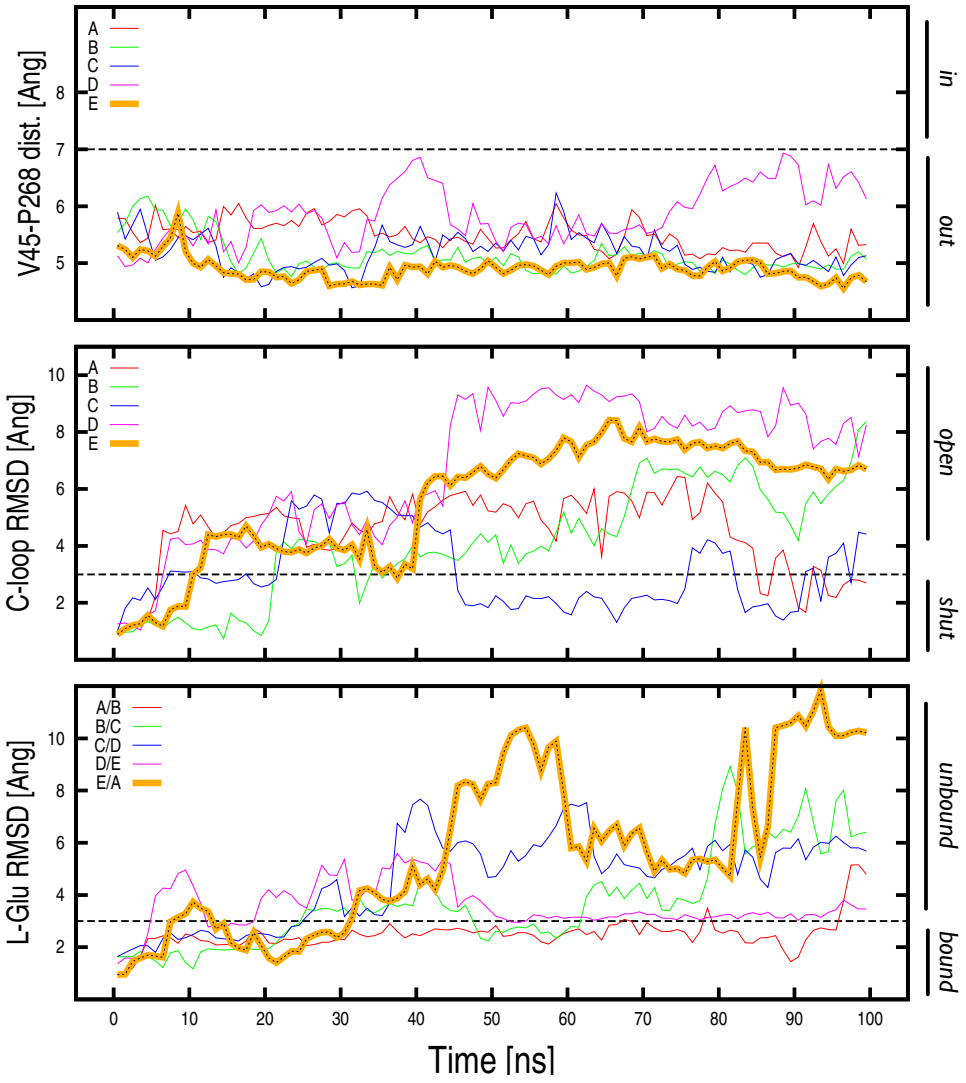

FIG. S11: Binding of the allosteric agonist ivermectin impairs the structural communication between the orthosteric agonist site and the loops at the EC/TM domain interface. From top to bottom, the time series of the distance between V45 (on β_1-β_2 loop) and P268 (on the M2-M3 loop), the C_α-RMSD of the C-loop from the X-ray structure, and the all-atom RMSD of L-glutamate from its active binding mode are shown as computed along the control simulation of GluCl with ivermectin present. Threshold values of 7 Å for the V45-P268 distance, 3 Å for the C-loop RMSD, and 3 Å for the L-glutamate RMSD were used to distinguish, respectively, the *out* from the *in* position of P268, the *shut* from the *open* conformation of the C-loop, the *bound* from the *unbound* state of L-glutamate; see black dashed lines. The data show that despite the opening of the C-loop and the unbinding of L-glutamate from the orthosteric site in two out of five subunits, no inward displacement of the M2-M3 loop is sampled on the simulation timescale; see subunit E (orange thick lines) for illustration. This suggests that the binding of ivermectin breaks the coupling between the orthosteric site and the interfacial loops of GluCl. As ivermectin stabilizes the untwisted conformation of the ion channel (see Figure 2 in *Main Text*), the latter indicates that a global twisting of the receptor is required for the allosteric communication between the EC and TM domains in pLGICs.

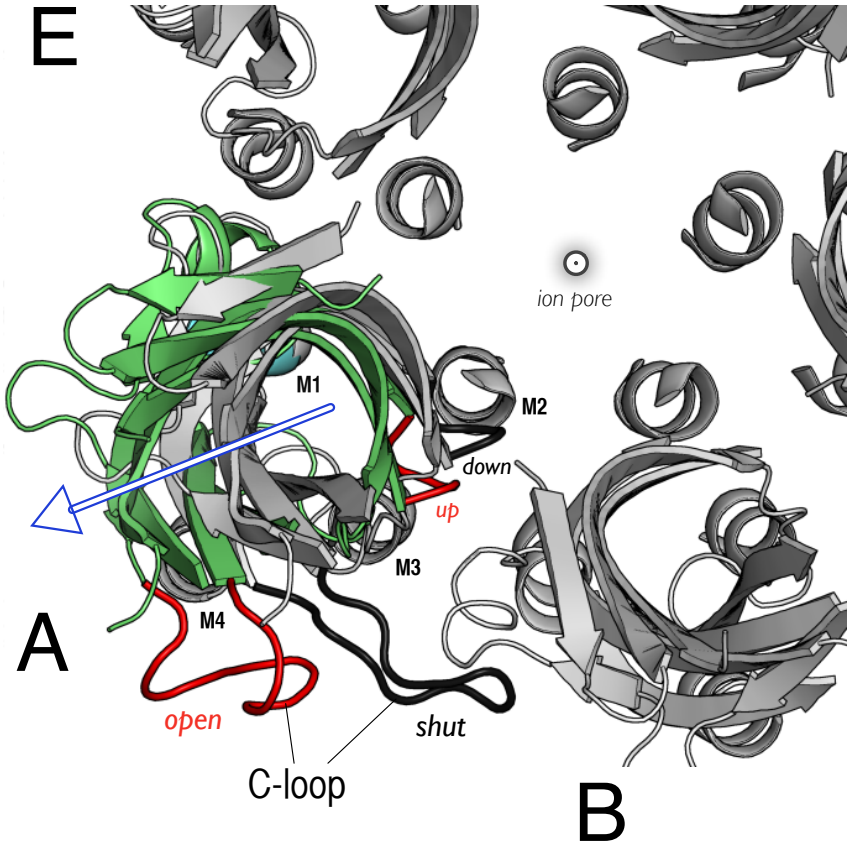

FIG. S12: Top view of the outward tilting of the β-sandwich in the A subunit sampled during the simulation of GluCl with ivermectin removed. The structural core of the ion channel at the beginning and after the spontaneous unbinding of L-glutamate from the (+) subunit is shown in tones of gray and colors, respectively. The structures were superposed on the TM domain to project out structural changes due to twisting. The comparison shows that the reorientation of the β-sandwich occurs in the direction of M4 (i.e., *outwards*) along the radial component; see the large arrow. A similar tertiary change is observed in the D subunit; see *Main Text*.

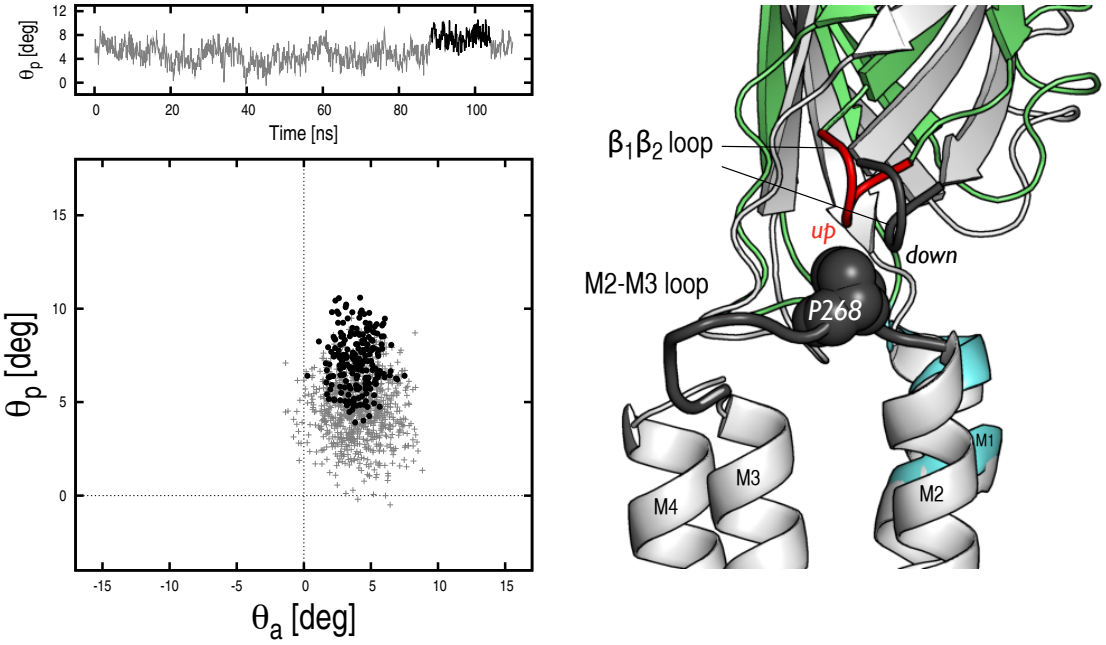

FIG. S13: The outward tilting of the β-sandwich in the EC domain as visualized in subunit D. On the left-hand side, the orientation of the β-sandwich is monitored by measuring both polar (θ_p) and azimuthal (θ_a) tilting components over time, as done in Figure 5 of the *Main Text*. The polar tilting of the β-sandwich shows a 4° increase between 88 and 110 ns; see black line and dots. Remarkably, such an outward tilting transition (∼88 ns) occurs when L-glutamate unbinds from the (+) subunit at the D/E interface; see Figure S10. Also, at ∼110 ns, the β-sandwich moves back to the initial *untilted* conformation as a consequence of agonist rebinding. On the right-hand side, the structural rearrangement of the D subunit in response to agonist unbinding/rebinding is illustrated by comparing snapshots taken at the beginning (gray scale) and 104 ns (in colors); structures were aligned by superimposing the TM region. As discussed for subunit A (see *Main Text*), the outward tilting of the β-sandwich results in the repositioning of the β_1-β_2 loop at the EC/TM domain interface, which moves from *down* to *up*. The repositioning facilitates the passage of the bulky side chain of P268 in the direction of the ion pore, thus coupling the orthosteric site in the EC domain to the ion pore in the TM domain.